Dual-Modality Imaging of Function and Physiology

Bruce H. Hasegawa[a], Koji Iwata, Kenneth H. Wong, Max C. Wu, Angela Da Silva[b], H. Roger Tang[c], William C. Barber, Andrew B. Hwang, Anne E. Sakdinawat

UCSF Physics Research Laboratory, University of California, San Francisco
Bioengineering Graduate Group, University of California, San Francisco
and University of California, Berkeley

ABSTRACT

Dual-modality imaging is a technique where computed tomography or magnetic resonance imaging is combined with positron emission tomography or single-photon computed tomography to acquire structural and functional images with an integrated system. The data are acquired during a single procedure with the patient on a table viewed by both detectors to facilitate correlation between the structural and function images. The resulting data can be useful for localization for more specific diagnosis of disease. In addition, the anatomical information can be used to compensate the correlated radionuclide data for physical perturbations such as photon attenuation, scatter radiation, and partial volume errors. Thus, dual-modality imaging provides *a priori* information that can be used to improve both the visual quality and the quantitative accuracy of the radionuclide images. Dual-modality imaging systems also are being developed for biological research that involves small animals. The small-animal dual-modality systems offer advantages for measurements that currently are performed invasively using autoradiography and tissue sampling. By acquiring the required data noninvasively, dual-modality imaging has the potential to allow serial studies in a single animal, to perform measurements with fewer animals, and to improve the statistical quality of the data.

Keywords: Dual-modality imaging, PET/CT, SPECT/CT, small animal imaging

1. INTRODUCTION

Medical diagnoses commonly rely on an assessment of both the functional status and the anatomical condition of the patient. In a clinical setting, *in vivo* measurement of organ physiology, tissue metabolism, tissue perfusion, and other biological functions can be performed with radionuclide-tracer techniques including positron emission tomography (PET) and single-photon emission computed tomography (SPECT). However, the visual quality and quantitative accuracy of radionuclide imaging is limited by some important physical perturbations[1]. Radionuclide images often lack anatomical cues that are needed to localize or stage the disease and typically are produced with poorer statistical and spatial characteristics than anatomical imaging methods such as computed tomography (CT) and magnetic resonance imaging (MRI). When physiological function is measured with radionuclide imaging, accuracy can be compromised by spatial resolution and photon-statistical limitations and by the need for attenuation correction and scatter compensation[1], for imaging with both single-photon and positron-emitting radionuclides.

These limitations have motivated the development of new approaches which combine functional data from SPECT or PET with structural data from MRI or CT. Researchers have investigated stereotactic techniques[2] or computer processing methods correlating functional information from SPECT or PET images with morphologic information from MRI or CT[3]. These techniques are most successful for imaging the head, where the rigidity of the skull allows anatomical and physiological images to be correlated using coordinate transformations applied in software. The situation is more complex when trying to correlate functional and structural images in the thorax or abdomen; since the body can bend and flex, simple rigid body coordinate transformations cannot be applied, especially when the two image sets are acquired on separate scanners over two different imaging sessions.

[a] bruceh@itsa.ucsf.edu; phone 1 415-502-4494; fax 1 650 742-0146; UCSF Physics Research Laboratory, 389 Oyster Point Blvd., Suite 1, South San Francisco, CA 94080.
[b] Currently at ADAC Laboratories, 540 Alder Drive, Milpitas, CA 95035
[c] Currently at Signature Biosciences, 21124 Cabot Blvd., Hayward CA 94545

Medical Imaging 2002: Physiology and Function from Multidimensional Images, Anne V. Clough, Chin-Tu Chen, Editors, Proceedings of SPIE Vol. 4683 (2002) © 2002 SPIE · 1605-7422/02/$15.00

Combined functional-radionuclide and anatomical-transmission imaging also has the potential to solve a different problem, that of overcoming the quantitative errors in radionuclide imaging, most notably those due to photon attenuation. Commercially available radionuclide imaging systems now are equipped with apparatus to acquire transmission scans of the patient with external radionuclide sources[4]. The transmission data are reconstructed to generate a patient-specific map of attenuation coefficients for attenuation correction of the radionuclide image. This technique is used to improve the quality myocardial perfusion imaging[5], but also has potential applications for tumor imaging where internally administered radiopharmaceuticals are being pursued for diagnosis and treatment of cancer.

To facilitate the process of correlating structural and functional information, and for improving the quantitative accuracy of radionuclide data, several investigators have developed a new class of diagnostic instrumentation that combine x-ray and radionuclide imaging. This approach is performed with medical imaging systems that perform anatomical imaging with CT, and functional imaging with SPECT or PET. These "dual-modality" systems use separate detectors for x-ray and radionuclide imaging. The detectors are integrated on a common gantry in a way that facilitates patient handling, data acquisition, and coregistration of the CT and radionuclide image data. Since CT can be used to generate a patient specific map of attenuation coefficients with a high degree of accuracy and precision, these systems also can be used to improve the quantitative accuracy of the radionuclide data for functional assessments. Therefore, the goal of these dual-modality imaging systems is to correlate function and structure, and to improve quantitation of radiopharmaceuticals using a noninvasive technique that is applicable for functional studies in a clinical setting. Quantitative radionuclide imaging would be important for assessing myocardial perfusion[6]. For example, the quantitation of myocardial blood flow and coronary reserve could provide a very sensitive therapeutic end-point for treatment of patients with risk factors, (e.g., elevated LDL cholesterol), and overall would provide a more rational basis for assessing metabolic function and coronary disease. Quantitative radionuclide assessments also would be important for clinical assessment of cancer[7,8] by allowing accurate perfusion measurements, precise localization of receptor-binding, and quantitative uptake measurements of therapeutic agents labeled with single-photon radionuclide such as iodine-131. These methods would improve the application of radionuclide imaging for tumor localization, metabolic assessments to stage the malignancy, tumor dosimetry for treatment planning and monitoring, and evaluating therapeutic response to surgery, radiation treatment, or chemotherapy[7,9,10].

2. CLINICAL IMPLEMENTATION

2.1 Design and Implementation of Dual-Modality Imaging Systems

The conceptual design of dual-modality imaging systems is quite simple. A typical dual-modality imaging has a CT scanner (x-ray tube and detector) and a radionuclide detector (PET or SPECT) mounted on a common gantry with a common patient table for x-ray and radionuclide imaging. X-ray CT scans and radionuclide scans are acquired by translating the patient from one detector to the other while the patient remains on the patient table. This allows the two image sets to be acquired with a consistent scanner geometry and body habitus, and with minimal delay between the two acquisitions. Virtually all dual-modality imaging systems separate the x-ray components from the radionuclide detector by 50 to 100 cm to insure that the high flux rate of x-rays generated during the CT acquisition do not damage the radionuclide detector. After both sets of images are acquired and reconstructed, image registration software[11] then is used to fuse the x-ray and radionuclide images in a way that accounts for differences in reconstruction diameter, offsets in isocenter, image reconstruction coordinates, and image format (e.g., 128×128 vs. 512×512). Over the past decade, PET/CT and SPECT/CT systems have been developed by academic researchers, most notably at the University of Pittsburgh and at the University of California, San Francisco (UCSF). More recently, commercial dual-modality imaging system have become available from the major medical imaging companies, including systems from GE Medical System, Siemens Medical Systems and CTI Incorporated, and Philips/ADAC Medical Imaging Systems. Finally, dual-modality systems for imaging small animals are being developed in both academic and corporate settings, and are discussed in Section 4 of this manuscript. Table 1 shows a list of several dual-modality systems that have been developed or that are under development. This list is not exhaustive, but tabulates the characteristics of several dual-modality imaging systems for different applications, including prototype evaluation, clinical use, and research involving small animal imaging.

2.2 PET/CT Imaging Systems

At the University of Pittsburgh, Townsend, Beyer, et al.,[19,20,22] implemented the first combined PET/CT ("SMART") system by combining a ECAT ART PET system from CTI Incorporated with a Somatom AR.SP spiral CT scanner. The ECAT ART uses a partial ring of BGO detectors that are mounted on a common rotating stage with the x-ray tube and detectors from a Somatom AR.SP spiral CT scanner. The PET and CT components can be operated either separately or in a combined mode, with the centers of the two tomographic systems offset by 60 cm. The PET subsystem includes 24 detector rings with a plane spacing of 3.375 mm. The CT subsystem operates at a maximum of 130 kVp and 105 mA, with scan times of 13 and 1.9 sec per slice, slice thicknesses of 1, 2, 3, 5, and 10 mm and in-plane spatial resolution of 0.45 mm and 6.2 mm respectively for the CT and PET images. Attenuation correction[21] of the PET data can be implemented by scaling the CT transmission image from its effective energy of 70 keV to 511 keV using hybrid

Table 1: Dual-Modality Imaging Systems

Year	Scanner Name/Type	Developer	Application	Radionuclide Detector	Description	References
1989, 1992	Emission-Transmission CT	UCSF	Phantoms, Animals	HPGe array	Pulse-counting detector, simultaneous SPECT/CT	12-16
1992	SPECT/CT	UCSF	Research, Clinical SPECT CT System	NaI(Tl), PMT (Scintillation Camera)	Separate CT, SPECT; Common patient table	11,17, 18
1998	PET/CT	Univ of Pittsburgh	Research, Clinical PET/CT system	BGO, PMT	BGO detector, CT; Common slip ring	19-22
1999	Discovery VH ("Hawkeye")	GE Medical Systems, Elgems Ltd	Clinical SPECT/CT System	NaI(Tl), PMT (Scintillation camera)	Scintillation camera, CT; Common slip ring	23-25
2000	Biograph	Siemens Medical, CTI Inc	Clinical PET/CT System	BGO, PMT	PET; spiral CT	
2000	Discovery VI ("Positrace")	GE Medical (SMV Medical)	Clinical PET/CT System	NaI(Tl), PMT	PET; spiral CT	
2001	Discovery LS	GE Medical	Clinical PET/CT System	BGO, PMT	PET; spiral CT	
2002	Gemini (under development)	Philips Medical, ADAC	Clinical PET/CT System	GSO, PMT	PET; spiral CT	
2000	PET/MRI	UCLA, UC Davis	Small animal	LSO, PSPMT	LSO detector in MRI; PSPMT readout	26-29
2001	PET/CT	UCLA, UC Davis	Small animal	LSO, PSPMT	LSO with PSPMT; CCD x-ray detector	30
2002	PET/CT	Forschungszentrum Jülich	Small animal	YAP, PSPMT	YAP with PSPMT; aSi:H x-ray detector	31
2000	SPECT/CT	Univ of Virginia	Small animal	CsI(Tl), PSPMT	CsI(Tl), PSPMT; CCD x-ray detector	32
2002	SPECT/CT	Photon Imaging, Inc.	Small animal	CsI(Tl), PSPMT	CsI(Tl), PSPMT; CMOS x-ray detector	
2002	SPECT/CT (under development)	UCSF	Small animal	CsI(Tl), Si-PD	CsI(Tl), Si-PD; CCD x-ray detector	33

Abbreviations: BGO bismuth germanate; CMOS complementary metal-oxide semiconductor; CsI(Tl) thallium-activated cesium iodide; HPGe high-purity germanium; NaI(Tl) thallium-activated sodium iodide; GSO gadolinium orthosilicate; LSO lutetium orthosilicate; PMT photomultiplier tube(s); PSPMT position-sensitive photomultiplier tube(s); Si-PD silicon photodiode(s); YAP yttrium aluminum perovskit

segmentation and scaling, with CT-based scatter correction performed prior to attenuation correction. The system has been used to image oncology patients covering a range of different cancers, including lung, esophageal, head and neck, melanoma, lymphoma, pancreas, and renal cell[22]. The aligned PET and CT images are used both for diagnosing and staging disease and for evaluating response to therapy.

More recently, several PET/CT scanners have been developed or are under development by commercial vendors for clinical utilization. In 2000, SMV Incorporated introduced a combined PET/CT scanner that incorporates a NaI(Tl) scintillator-based PET scanner and a spiral CT scanner integrated with a common patient table for combined PET/CT imaging. The system now is available as the "Discovery VI" from GE Medical Systems. In 2001, both Siemens Medical Systems and GE Medical Systems introduced high-performance PET/CT scanners with stationary BGO detectors capable of three-dimensional PET imaging and multislice spiral CT scanner. Finally, Philips Medical System is developing a PET/CT scanner having a gadolinium orthosilicate (GSO) detector for PET imaging that is integrated with a dual-ring spiral CT scanner. PET/CT scanners with lutetium orthosilicate (LSO) detectors now are under development at CTI Incorporated and Siemens Medical Systems, and offers the potential for higher count-rate capabilities and faster scan times especially for three-dimensional PET imaging.

2.3 SPECT/CT Imaging Systems

In comparison to the development effort at the University of Pittsburgh, researchers at the UCSF Physics Research Laboratory have pioneered the development of dual-modality imaging systems that combine x-ray computed tomography (CT) and single-photon emission computed tomography (SPECT). The first dual-modality imaging system developed at UCSF[13] had a 20 cm reconstruction diameter for imaging phantoms and animals. The system used a segmented high-purity germanium (HPGe) detector operated in a fast photon-counting mode[34] with sufficient energy resolution to discriminate x-ray photons from an external source (for computed tomography) from emission γ-rays from an internal radionuclide source. The system was used for imaging studies in phantoms and in animals with ^{99m}Tc-sestamibi in a porcine model of myocardial perfusion[15,16,35,36].

As an outgrowth of initial studies with the prototype dual-modality system described above, the UCSF group also developed a combined CT/SPECT system[11] for clinical studies. The system was configured by siting a scintillation camera (GE 600 XR/T) adjacent to a commercial CT scanner (GE 9800 Quick), allowing the patient to be scanned first in the CT scanner, then moved into the SPECT system by simple translation of a common patient table.

As an example, SPECT images obtained from a 7-year old female with neuroblastoma, five days after therapeutic intravenous administration of 364 mCi of ^{131}I-mIBG (18 mCi/kg) are shown in Fig. 1. Tomographic radionuclide data were acquired at 64 views over 360°, 15 s/view, with a count rate of approximately 10 kcps using a high-energy general-purpose collimator. CT images were obtained without iodinated contrast at 140 kVp, 70 mA, 2 s/slice in a 512 × 512 format. The SPECT images were reconstructed with filtered backprojection (Fig. 1 left), with 100 iterations of an ML-EM algorithm including attenuation correction and compensation for the geometric response of the collimator (Fig. 1 middle), and with the correlated CT image of the same anatomical region (Fig. 1 right). These images show that at-

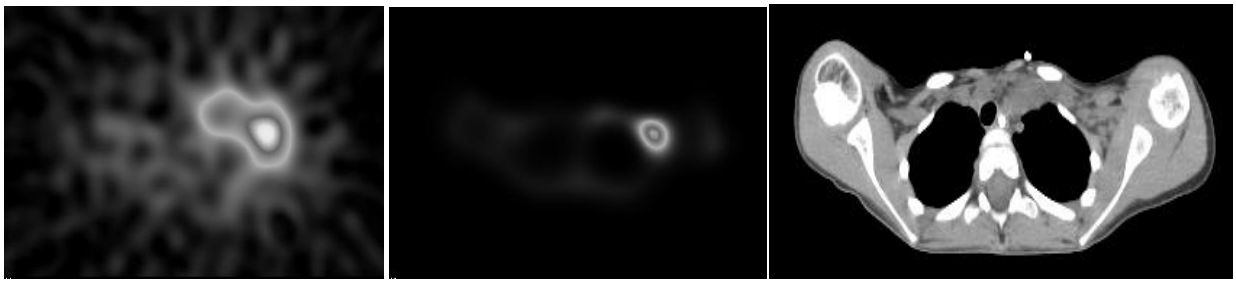

Figure 1: SPECT images of a neuroblastoma patients showing radionuclide reconstruction with filtered-backprojection (left), radionuclide reconstruction using ML-EM algorithm including compensation for photon attenuation and collimator response (middle), and correlated CT image (right)

tenuation correction and compensation for collimator response significantly improve delineation of radionuclide uptake in comparison to more conventional reconstruction methods (e.g., filtered backprojection) that are still in common clinical use.

GE Medical Systems (Milwaukee WI) and Elgems Ltd (Haifa Israel) have developed a dual-modality imaging system that includes a low-resolution CT capability[23-25]. The system includes two rectangular scintillation cameras with NaI(Tl) crystals mounted on a slip ring to perform radionuclide tomography. The radionuclide detectors can be operated with conventional collimators for planar scintigraphy or SPECT, and also perform coincidence detection of annihilation photons for imaging ^{18}F-fluorodeoxyglucose and other positron-emitting radionuclides. An x-ray tube (140 kVp, 2.5 mA) and x-ray detector array having 384 elements each 1.8×2.8 mm^2 also are mounted on the same slip ring to perform x-ray tomography. The resulting anatomical images are generated with a spatial resolution of 2.5 mm FWHM in plane[25] and with a 1 cm mid-plane slice width. The CT image can be used for anatomical localization of the radionuclide data, and also can be calibrated to the energy of the radionuclide photon for photon correction of the radionuclide image. Transmission scanning is obtained with a scan time of approximately 20 sec per slice with a 40-cm diameter axial field of view for both radionuclide and x-ray imaging.

Finally, investigators at the University of Virginia[37] have developed a dual-modality breast imaging system. The system incorporates six charge-coupled device modules tiled together to enable full-field digital mammography with a spatial resolution of 46 microns. Planar radionuclide imaging of ^{99m}Tc-sestamibi (Miraluma, DuPont Pharma) is performed with a 4×4 array of position-sensitive photomultiplier tubes coupled to an array of 3 mm square CsI(Tl) scintillator crystals. Fusion of the structural and functional is performed without fiducial markers using the known geometrical relationship between the x-ray and radionuclide planar images in the way that assists in the interpretation of radiopharmaceutical uptake in the nuclear medicine image.

3. RADIONUCLIDE QUANTIFICATION

3.1 Measurement of Physiology Function with Radionuclide Imaging

Nuclear medicine offers the potential to measure regional radiopharmaceutical uptake to assess physiological function in the intact animal or human. Nuclear medicine also offers exquisite detection sensitivity, allowing the radiopharmaceutical to be administered and measured in tracer amounts. Therefore, the measurement can be performed noninvasively without perturbing the function of the physiological system being monitored. Conventional methods to quantify radionuclide images use regions of interest that are defined directly on the radionuclide image itself. This approach, however, has several drawbacks. First, radionuclide images inherently lack anatomical information in a way that can frustrate the reliable definition of object boundaries, particularly in low count rate images. Furthermore, physical perturbations occur during the imaging process (photon attenuation, scatter, and partial volume effects) that can severely affect the accuracy of the quantitation process. Compensating the radionuclide image reconstruction process for physical errors can lessen these effects, but it is not possible to recover all of the information that is lost in the imaging process by processing the radionuclide image alone.

While current attention on dual-modality imaging systems has focused on their ability to improve registration of radionuclide and CT images, they also have the potential to improve the accuracy of quantitative radionuclide measurements. This is achieved in several ways. First, dual-modality imaging provides an anatomical image from CT can that be used as a template to define anatomically-specific regions of interest to quantify radionuclide uptake in the correlated PET or SPECT images. Second, *a priori* anatomical information from CT can be used to generate an object-specific map of attenuation coefficients, scatter coefficients, or recovery coefficients to correct the radionuclide data for errors due to photon attenuation, scattered radiation, or partial volume errors. Therefore, correlated x-ray and radionuclide data from dual-modality imaging provides the potential to improve the quantitative accuracy of functional measurements in comparison to measurements extracted solely from the nuclear medicine study.

3.2 Photon Attenuation

All nuclear medicine data, including PET, suffer from errors due to “photon attenuation” in which gamma rays

emitted by the radiopharmaceutical are absorbed by overlying anatomical structures. It is possible to compensate the radionuclide data for these errors using a patient specific map of linear attenuation coefficients derived from the co-registered CT image acquired from the patient. At UCSF, the calibration of the patient-specific images to units of linear attenuation coefficient is performed using calibration measurements[11] obtained from a phantom with inserts containing water, fat-equivalent (ethanol), and bone equivalent material (K_2HPO_4). CT scans of the calibration phantom are obtained at the same technique (kV, mAs, slice width, etc). CT numbers then are extracted from each region and are plotted against their known attenuation coefficients. This generates calibration data[11,38,39] that are used to transform the patient specific CT images from Hounsfield units to units of linear attenuation coefficient (cm^{-1}) for the photon energy of the radionuclide. The attenuation map then is incorporated into an iterative (e.g., maximum likelihood expectation maximization) algorithm for reconstruction of the radionuclide data to compensate the radionuclide data for photon attenuation in the radionuclide image. Correction techniques for photon attenuation using correlated x-ray CT images now have been developed and implemented for both PET/CT and SPECT/CT systems[21,22,24,25].

3.3 Scatter Radiation

In addition to photon attenuation, Compton scatter can perturb and introduce errors into the nuclear medicine image. Several techniques that have been reported in the literature that can estimate the magnitude of scatter in the radionuclide image. For example, the "Compton window" method which estimates the scatter from a fraction of the counts recorded in an energy window placed away from the photopeak[40,41]. Alternatively, the "dual photopeak window method" which estimates the scatter-to-primary ratio from a third-order polynomial of the ratio between the counts recorded in two energy windows symmetrically placed around the photopeak[42,43]. Finally, the "convolution-subtraction method"[44,45] which estimates the scatter contribution by convolving the detected data with an appropriate "scatter point spread function"[46,47]. Recently, several investigators have developed scatter estimation methods[48,49] based on the concept of defining an effective source distribution of scatter photons, and calculating the expected scatter projection data from this effective source. The method approximates the scatter from a primary source by convolving the primary source distribution with a kernel (or point spread function) that is calculated (using Monte Carlo techniques) from a point source in an infinite water medium to estimate the "effective" source of detected scatter photons. Assuming spatial invariance and to first order, the scatter distribution, *s(t)*, is estimated as[48]:

$$s(t) = \mathrm{Proj}\{\rho(x')[a(x') * k_n(x')]\} \qquad (1)$$

where $\rho(x')$ is the electron density at x' relative to water, $a(x')$ is the estimated activity concentration, * represents the three-dimensional convolution operation, and where "*Proj*" is an operator that simulations projection of the radionuclide data onto the radionuclide detector. The kernel $k_n(x')$ is the product of (a) the probability that a photon is scattered at x' after traveling via any possible path from its point of emission at the coordinate system origin, (b) the probability that photon's energy is within the energy discrimination window of the imaging system, and (c) the probability that the photon is scattered in the direction of the detector, and can incorporate a patient specific map of linear attenuation coefficients derived from CT. These kernels can be efficiently calculated for a specific imaging geometry using Monte Carlo methods[50] as Frey has done for the case of parallel hole collimators[48].

3.4 Collimator Response

Nuclear medicine is characterized by spatial resolution limitations that are more severe than those obtained in anatomical imaging. For example, methods such as computed tomography (CT) and magnetic resonance imaging (MRI) can image details having a size dimension of one millimeter or smaller. In comparison, positron emission tomography offers spatial resolution in the range of 3 to 5 mm FWHM, while the spatial resolution of SPECT is in the range of 8 to 14 mm FWHM. The spatial resolution limitations of nuclear medicine obviously affects image quality by blurring small structures, thereby degrading detectability and reducing contrast with respect to background structures. The finite spatial resolution of nuclear medicine also can introduce significant errors in quantitative radionuclide measurements by partial volume averaging. Conceptually, spatial resolution losses in both planar and tomographic radionuclide imaging cause "spill-out" of the target activity into the background, and "spill-in" of the background activity into the target. Therefore, when a border is defined around an target region in a radionuclide image, the target activity often is contaminated with background activity blurred into the target region by spatial resolution losses of the imaging system. These errors can be compensated using "recovery coefficients" which represent correction factors for these partial volume errors[51]. When a

CT image is available that is correlated to a radionuclide image, then the actual size of the target can be estimated by defining a region of interest around the anatomical target region. The region of interest then can be used to estimate the magnitude of the partial volume error. The recovery coefficient then can be used to compensate the radionuclide values for these effects. The recovery coefficient method works well for simple geometries (e.g., spherical lesions) but is more difficult to apply for target regions that have a more complex shape.

3.5 Radionuclide Quantification

Recently, Tang et al.[52] developed compensation techniques that depart from the traditional paradigm of correcting the radionuclide images prior to quantitation by incorporating physical models, not in image reconstruction, but rather into the quantitation process itself. In this technique, regions-of-interest (ROI's) for the target (e.g., tumor) and background regions are defined on the high-resolution CT image for quantitation of the radionuclide data. Once the target and background volumes are defined on the high-resolution CT image, they are resampled and reoriented into the coordinates of the radionuclide image using the known geometrical transformation between the CT coordinate system and the scintillation camera coordinate system provided inherently by dual-modality imaging. The resulting regions represent idealized objects (e.g., tumor vs. background) containing unit radionuclide concentration. Then, using a realistic physical model of the imaging process that includes photon attenuation, non-ideal collimation, and other physical perturbations, the template is mathematically projected to simulate the acquisition of the radionuclide image.

Planar imaging of the ideal radionuclide objects is modeled by mathematically projecting the templates onto the plane of the radionuclide detector. This process generates "projected templates" that are analogous to conventional ROI's, in that the projected templates specify the geometry of the tumor and background regions on the projected planar radionuclide images; however the projected templates are defined on the high-resolution CT images rather than on the low-resolution radionuclide images. Furthermore, unlike traditional ROI's which are uniform, the projected templates are nonuniform and contain information about physical effects included in the projector model. There are several methods by which the projected templates can be used to quantify activity in the radionuclide image. If we assume that the image process is linear, and consider the photons emitted from M different regions (e.g., tumor, background) where each region has a uniform activity concentration A_m, then the counts $p(d)$ measured in detector (i.e., pixel) d is estimated by

$$p^*(d) = \sum_{m=1}^{M} A_m \phi_m(d) \tag{2}$$

where $\phi_m(d)$ represents the value of the projected template at detector location d, which is physically equivalent to the relative number of photons detected from radioactive region m in pixel location d. If we measure the value $p(d)$ from the planar emission data and given that we have calculated $\phi_m(d)$ from the template-projection technique, we can estimate the activity concentration A_m for region m (i.e., for the target lesion) by minimizing the weighted least squares difference

$$\chi^2 = \sum_{d=1}^{D} \left[\frac{p(d) - \sum_{m=1}^{M} A_m \phi_m(d)}{\sqrt{p(d)}} \right]^2 \tag{3}$$

where D is the number of detectors elements (i.e., pixels) from which we estimate the activity concentrations (typically an area surrounding the target lesion). We note that a theoretical basis for this formulation has been described elegantly by Formiconi[53] and is similar to a method described by Liu[54]. An alternative formulation assuming Poisson statistics was suggested by Carson[55]. Specific details of our implementation can be found in the doctoral dissertation completed by Tang[52].

The template projection technique described above for planar imaging can be extended to quantify target regions in tomographic images[52]. This technique begins by repeating template projection for all angles sampled by the tomographic acquisition of the real radionuclide data. The original template, defined on the high-resolution CT image, specifies the geometry for the volume of interest in the radionuclide image. After the template projection data are modeled for the target and for the neighboring objects, they are reconstructed with the same reconstruction algorithms (e.g.,

ML-EM or filtered-backprojection) used for reconstructing the emission data. The reconstructed templates contain information about physical effects (e.g., photon attenuation, scattered radiation) included in the modeling process and can be used to quantify the emission tomographic data. Several methods are then available for estimating the object activity concentration. For example, the radionuclide content $\rho(i)$ of the target region can be calculated using a technique analogous to Eq. (2) for planar imaging by assuming that both the imaging and reconstruction processes are linear. Alternatively, the corrected mean activity concentration ρ_t in the target region can be calculated by voxel-by-voxel rescaling after estimating or assuming the background activity concentration ρ_b

$$\rho_t = \frac{1}{N}\sum_{i=1}^{N}\frac{\rho(i) - \rho_b\gamma_b(i)}{\gamma_t(i)} \tag{4}$$

where $\gamma_b(i)$ and $\gamma_t(i)$ represent the reconstructed template values for voxel location i and contributed by the background (b) and target (t) regions respectively. The voxel-by-voxel correction is analogous to scaling the reconstructed data with object size- and shape-dependent recovery factors[8,51]. Therefore, multiplicative errors caused by photon attenuation and other perturbations are compensated in Eq. 3 by division by $\gamma_t(i))$ and while "spill-in" of background activity into the target lesion is corrected by subtraction of the term $\rho_b\gamma_b(i)$. The radionuclide content of a given target region t, can be calculated as $\rho_t V_t$ where V_t is the actual target volume defined on the CT image.

3.6 Experimental Studies

Da Silva et al[17] have tested the radionuclide quantitation techniques described above in a porcine model of myocardial perfusion using radionuclide imaging of ^{99m}Tc-sestamibi with the CT/SPECT system at UCSF. The study was performed to test the accuracy of radiopharmaceutical content measured noninvasively against corresponding values measured directly from excised tissue samples. All studies were performed with the animals under general anesthesia, with mechanical ventilation, and with ECG monitored continuously. Catheters were placed in an ear vein for dipyridamole (a vasodilator) infusion, administration of normal saline, and for injection of ^{99m}Tc sestamibi. In some animals the proximal LAD was isolated and occluded until ST-interval changes were confirmed using surface EKG electrodes. The ribs then were reapproximated for closed-chest imaging simulation. Individual animals were imaged in one of four different perfusion states: (a) with neither coronary occlusion nor dipyridamole infusion, (b) with coronary occlusion alone, (c) following dipyridamole infusion alone, and (d) with both coronary occlusion and dipyridamole infusion.

Prior to imaging, the animals were administered approximately 30 mCi of ^{99m}Tc-sestamibi for radionuclide evaluation of myocardial perfusion. Thoracic projection x-ray scans were obtained using the CT system to localize the mid-left ventricular levels. The animals were administered nonionic iodine contrast media, and were positioned supine in the imaging system to obtain thoracic CT images across the extent of the left ventricle. CT imaging was followed by radionuclide (SPECT) imaging of the same anatomical region for correlation with the CT scans. After the animal was euthanized, its heart was removed, flushed, and sectioned. The radionuclide image was reconstructed and "template projection-reconstruction" (see Section 3.5) was used to quantify radionuclide uptake in 15 to 20 regions corresponding to those obtained directly from the excised tissue samples.

Regional measurements of myocardial ^{99m}Tc-sestamibi uptake comparing values obtained from excised tissue samples (*ex vivo*) were compared those obtained with CT/SPECT using template projection-reconstruction (*in vivo*). The data points (*in vivo* vs. *ex vivo*) were fit to a line using linear regression and ideally should fall along the line of identity with unit slope. However, the *in vivo* values generated with neither attenuation correction nor correction for partial volume errors had a slope of roughly 0.1, thereby representing an order-of-magnitude error in comparison to *ex vivo* values. In comparison, *in vivo* values obtained with attenuation correction alone had a slope of 0.42 (absolute error of –55%), while those obtained with both attenuation correction and with compensation for collimator response (using template projection-reconstruction) were generated with an absolute accuracy error of approximately –10%. This demonstrates the improved accuracy of *in vivo* radionuclide quantification obtained using dual-modality for assessment of myocardial perfusion, as an example of how dual-modality imaging can be used to assess physiological function with radiopharmaceuticals.

4. SMALL ANIMAL IMAGING

4.1 Need for Small Animal Imaging

Initial interest in dual-modality imaging has centered on the need to improve diagnosis and evaluation of patients in a clinical setting. However, increasingly researchers are pursuing the development of specialized dual-modality systems for imaging small animals in a research setting. Biomedical researchers have long used animal models to investigate mechanisms and treatment of human diseases. In part, this has been motivated by the availability of modern transgenic and knockout techniques[56,57] that have produced animals in which selected genetic alterations can define the disease phenotype. Trangenic animal models now affect research in every area of biomedical science[56] including the neurosciences[58,59], behavior[60], pharmacology [61], anesthesia and addiction[62], molecular biology, mutagenesis, and carcinogenesis[61,63]. The availability of transgenic animals facilitates the development of therapeutic techniques, including the use of drugs and antibodies[57]. Similarly, advances in transgenic approaches have produced genetically engineered mice[64] that are being used in experimental studies to improve our understanding of mammalian cardiovascular development, differentiation, function, and disease[64]. It is clear from these examples that transgenic animal technology now has an essential role and profound influence in all areas of biomedical research.

The innate physical characteristics of mice both facilitate and complicate their use as a model for biological research. For example, mice are genetically similar to humans, have short reproductive cycle, and are relatively easy to house and maintain in a laboratory setting. However, a mouse's small size (about 15-40 grams), heart rates of around 600 beats per minute), and rapid metabolic rates complicates *in vivo* functional measurements[64-66]. Autoradiography or tissue sampling can be used to quantify the tissue distribution of radiotracers for functional assessments with excellent spatial resolution (10 to 100 μm)[67,68]. However, these techniques are invasive, require the animal to be sacrificed, are labor intensive, and do not allow serial studies to be performed in the same animal. Therefore, high resolution imaging techniques would provide an important tool for small animal research, and is especially critical for studies where noninvasive functional assessments are needed.

Several investigators have developed high-resolution techniques suitable for noninvasive imaging of small animals. Anatomical studies can be performed using high-resolution magnetic resonance imaging. Similarly, magnetic resonance spectroscopy[65] can be used to assay the regional concentrations of metabolites. High-resolution x-ray CT (down to approximately 10 microns) has been developed for anatomical imaging studies[69,70]. Several investigators[71-75] are developing dedicated PET systems with sufficient spatial resolution (1 to 2 mm) for imaging small animals. Increasingly, these instruments are being used for metabolic studies with ^{18}F-fluorodeoxyglucose, and to assess pharmacokinetic and pharmacodynamic events in the early stages of drug development[76]. Other laboratories[77-84] have investigated pinhole imaging techniques to produce radionuclide images with spatial resolutions (1 to 2 mm) suitable for studies in small animals. Barrett, Barber et al.[85,86] are developing a high-resolution semiconductor detector and read-out system for single-photon imaging with spatial resolution and detection efficiencies suitable for studies on small animals.

4.2 Small Animal PET/CT and PET/MRI Systems

Several investigators are developing dual-modality systems that combine positron emission tomography (PET) with computed tomography (CT) or magnetic resonance imaging (MRI) at length scales suitable for small animal imaging. These developments are motivated by several reasons that are similar to those motivating the development of clinical dual-modality systems for imaging humans. First, while PET can provide important information for evaluating the metabolic state of various tissues (e.g., heart, brain) in the animal or for detecting tumors, the addition of anatomical imaging from CT or MRI helps to delineate anatomical/functional relationships needed for phenotyping and for other experimental protocols. The availability of dual-modality imaging also allows the possibility of defining regions of interest on the anatomical image, and for implementing corrections for photon attenuation and scatter radiation in a way that may improve quantitative analysis of the radionuclide data.

Goertzen, Cherry, et al.,[30] have developed a dual-modality system that combined microPET and microCT suitable for small animal imaging. MicroPET is implemented using LSO crystals that are coupled to position-sensitive photomultiplier tubes using an optical taper while microCT is implemented using a two-dimensional x-ray detector. The

microPET system offers a spatial resolution of approximately 2 mm FWHM, while microCT has a spatial resolution of approximately 100 μm FWHM. By shielding the radionuclide detector with metallic filters that absorb lower energy photons from the x-ray beam but allow transmission of the annihilation photons from the PET image, the system is capable of simultaneous microPET and microCT imaging. A similar approach is being implemented by Khodaverdi et al[31] who are using a two-dimensional amorphous silicon x-ray detector with a spatial resolution of 400 μm FWHM for CT. Both groups are implementing techniques for image registration and for deriving an object-specific map of attenuation coefficients from CT that can be used to correct the PET data for photon attenuation.

Shao, Slates, Cherry, et al., have developed a compact detector array, suitable for microPET imaging, that can be placed in an magnetic resonance imaging (MRI) system for simultaneous *in vivo* PET and MRI imaging of mice and rats[26-28]. The PET imager is configured as a 38 mm ring of lutetium oxyorthosilicate (LSO) crystals that are coupled via a 4 m long optical fibers to individual channels of a multi-channel photomultiplier tube (MC-PMT). The system is configured so that the PET detector can be placed in an MRI magnet while imaging the animal with the MC-PMT placed outside of the magnet where it can be shielded from the residual magnetic field of the MRI system. The system allows simultaneous PET and MRI imaging of small animals with pixel sizes of 0.313 mm and 0.938 mm for MRI and PET respectively. Ultimately, the goal of this work is to design a larger PET detector ring that can be used for simultaneous correlated PET/MRI imaging of the human brain.

4.3 Small Animal SPECT/CT Systems

The development of high-resolution gamma-ray detectors for small animal imaging has lead researchers at the Thomas Jefferson National Accelerator Facility (Jefferson Lab), the College of William and Mary[87] to implement this technology in a dual-modality CT/SPECT system for small animal imaging. The SPECT system uses position-sensitive photomultiplier tubes coupled to an array of CsI(Tl) scintillators. X-ray CT has been implemented using a compact fluoroscopy x-ray system with a 5 cm diameter field of view. Both the radionuclide detector as well as the x-ray source and detector are mounted on a gantry with 18 cm diameter rings for acquisition of the combined SPECT/CT tomographic images. The system is configured to image radionuclides with photon energies as low as 27 keV, making it feasible to image the Kα and Kβ x-rays (27-32 keV) and 35 keV gamma-ray from iodine-125, a radiotracer commonly used for autoradiography and *in vitro* counting of tissue samples in biological research. In addition, iodine-125 is relatively inexpensive, has a half-life of 59.4 days, and can be used to radiolabel antibodies and other biomolecules, making it an appealing agent for small animal research. A similar system incorporating CsI(Tl) scintillators and position-sensitive photomultiplier tubes, and a CCD-based x-ray detector and microfocus x-ray source has been configured by Williams et al[32] at the University of Virginia.

Photon Imaging Incorporated (Northridge CA) is developing a combined CT/SPECT system for dual-modality imaging of small animals. The radionuclide detector[88] uses an array of NaI(Tl) scintillation crystals coupled to position-sensitive photomultiplier tubes. The radionuclide detector provides submillimeter spatial resolution for pinhole-source distances suitable for tomographic imaging of mice when operated with a pinhole collimator having a 0.5 mm diameter aperture[89]. The anatomical data will be obtained with a CMOS x-ray detector and compact x-ray source to generate x-ray tomograms with a spatial resolution of 100 microns FWHM. In the current version, the animal is positioned vertically on a rotating stage with the x-ray and radionuclide detectors positioned to image the same object volume. A new gantry is under development, which will allow x-ray and radionuclide tomograms to be acquired with the animal placed in a stationary horizontal position.

At UCSF, we are developing a combined CT/SPECT system for small animal that will generate both functional (radionuclide) images and anatomical (x-ray) images, at spatial resolutions suitable for small animal imaging[33,90]. The systems integrate emission and x-ray imaging in a single device, and allow radionuclide uptake to be localized on a high-resolution CT image. Radionuclide imaging will be performed using silicon photodiode arrays coupled to a thallium-activated cesium iodide (CsI(Tl)) scintillator. The small animal imager also will incorporate a high-resolution x-ray CT system for imaging studies in small animals at spatial resolutions in the range of 100 μm, similar to those developed at other laboratories[69,70,91,92].

By providing a consistent method of correlating functional and structural information, combined CT/SPECT

imaging can improve both the accuracy and the precision of *in vivo* radionuclide measurements. The transmission data can be used to derive an attenuation map for attenuation compensation[12,15,38] to resolve regional nonuniformities for relative assessments with SPECT. Although the tissue lengths encountered in small animals are significantly shorter than those encountered in humans, errors due to photon attenuation may be significant when lower-energy radionuclides are used (e.g., 30 keV from ^{125}I) or when quantitative measurements are required. In addition, the small dimensions of small animals will exaggerate partial volume errors, but can be compensated using techniques such as the template-projection methods described above.

5. DISCUSSION AND CONCLUSIONS

Over the past 2 to 3 years, dual-modality imaging has emerged from development at academic and industrial centers, and now is undergoing the process of commercial dissemination and implementation in clinical settings. The primary benefit of these systems is that they facilitate fusion of anatomical and functional information by producing x-ray and radionuclide images of the patient in a consistent geometry. The first applications of dual-modality imaging will utilize the functional/structural correlation to improve cancer staging and to help in the delineation of normal versus abnormal uptake of radionuclide tracers. Dual-modality imaging also can provide patient specific anatomical information that can be used as *a priori* information to compensate radionuclide data for physical effects such as photon attenuation, scattered radiation, and partial volume errors. Therefore, dual-modality imaging has the potential to facilitate functional assessments using radionuclide imaging, especially for (but not limited to) heart disease and cancer, especially when quantitatively accurate measurements of radionuclide uptake would be desirable. Over the longer term, dual-modality imaging may find an increasing role for *in vivo* measurements of function and physiology of mice. Potential applications include those noted above, including the development of new radiopharmaceuticals, assessment of new therapeutic approaches, and investigation of fundamental biological processes in transgenic and knockout mice. These techniques would allow investigators to perform serial and repeat imaging studies in the same animal at multiple time points to investigate tumor growth, tissue pathology, the effects of therapy, and the mechanism of action of new diagnostic agents. Therefore, dual-modality combines high-resolution imaging capabilities and the potential for achieving accurate quantitation of radionuclide uptake in humans and in small animals. In this way, dual-modality imaging could have wide applicability and significant impact in clinical use of radionuclide imaging and in research that uses small animals to advance our understanding of human growth, development, and disease.

ACKNOWLEDGMENTS

The authors acknowledge support from NIH Grant 1 R01 CA50539, NIH Grant 1 R21 CA86893, NIH Subcontract N44 NS02305, NIH Grant R44 RR09859, NIH Grant 1 R01 CA91771, from the Department of Defense DAMD 17-98-1-8192. The authors also acknowledge a significant equipment grant from General Electric Medical Systems, and a gift from Cytogen Corporation.

REFERENCES

1. R. J. Jaszczak, R. E. Coleman, F. R. Whitehead, Physical factors affecting quantitative measurements using camera-based single photon emission computed tomography (SPECT). *IEEE Trans Nucl Sci*. **28**, pp. 69-80, 1981.
2. P. T. Fox, J. S. P. Perlmutter, M. E. Raichle, A stereotactic method of anatomical localization for positron emission tomograph. *J Comput Assist Tomogr*. **9**, pp. 141-153, 1985.
3. D. N. Levin, C. A. Pelizzari, G. T. Y. Chen, C. T. Chen, M. D. Cooper, Retrospective geometric correlation of MR, CT, and PET images. *Radiology*. **169**, pp. 817-823, 1988.
4. C. H. Tung, G. T. Gullberg, G. L. Zeng, P. E. Christian, F. L. Datz, H. T. Morgan, Non-uniform attenuation correction using simultaneous transmission and emission converging tomography. *IEEE Trans Nucl Sci*. **39**, pp. 1134-1143, 1992.
5. E. P. Ficaro, J. A. Fessler, P. D. Shreve, J. N. Kritzman, P. A. Rose, J. R. Corbett, Simultaneous transmission/emission myocardial perfusion tomography: Diagnostic accuracy of attenuation-corrected Tc-99m-sestamibi single-photon emission computed tomography. *Circulation*. **93**, pp. 463-473, 1996.
6. R. E. Patterson, S. F. Horowitz, R. L. Eisner, Comparison of modalities to diagnose coronary artery disease. *Semin Nucl Med*. **24**, pp. 286-310, 1994.

7. G. L. DeNardo, D. J. Macey, S. J. DeNardo, C. G. Zhang, T. R. Custer, Quantitative SPECT of uptake of monoclonal antibodies. *Semin Nucl Med*. **19**, pp. 22-32, 1989.
8. K. F. Koral, K. R. Zasadny, M. L. Kessler, J. Q. Juo, S. F. Buchbinder, M. S. Kaminski, I. Francis, R. L. Wahl, CT-SPECT fusion plus conjugate views for determining dosimetry in Iodine-131-monoclonal antibody therapy of lymphoma patients. *J Nucl Med*. **35**, pp. 1714-1720, 1994.
9. R. L. Nunnally, P. P. Antich, New directions in medical imaging of cancer. Magnetic resonance methods and single photon emission computed tomography. *Cancer*. **67**, pp. 1271-1277, 1991.
10. S. M. Larson, Radioimmunology. Imaging and therapy. *Cancer*. **67**, pp. 1253-1260, 1991.
11. S. C. Blankespoor, X. Wu, K. Kalki, J. K. Brown, H. R. Tang, C. E. Cann, B. H. Hasegawa, Attenuation correction of SPECT using x-ray CT on an emission-transmission CT system: Myocardial perfusion assessment. *IEEE Trans Nucl Sci*. **43**, pp. 2263-2274, 1996.
12. B. H. Hasegawa, J. K. Brown, T. F. Lang, S. M. Reilly, S. C. Liew, E. L. Gingold, C. E. Cann, Object-specific attenuation correction of SPECT with simultaneous x-ray CT. *IEEE Trans Nucl Sci*. **40**, pp. 1242-1252, 1993.
13. B. H. Hasegawa, E. L. Gingold, S. M. Reilly, S. C. Liew, C. E. Cann, Description of a simultaneous emission-transmission CT system. *Proc SPIE*. **1231**, pp. 50-60, 1990.
14. B. H. Hasegawa, S. M. Reilly, E. L. Gingold, C. E. Cann, Design Considerations for a Simultaneous Emission-Transmission CT Scanner. *Radiology*. **173(P)**, pp. 414, 1989.
15. K. Kalki, S. C. Blankespoor, J. K. Brown, B. H. Hasegawa, M. W. Dae, M. Chin, C. Stillson, Myocardial perfusion imaging with a combined x-ray CT and SPECT system. *J Nucl Med*. **38**, pp. 1535-1540, 1997.
16. T. F. Lang, B. H. Hasegawa, S. C. Liew, J. K. Brown, S. C. Blankespoor, S. M. Reilly, E. L. Gingold, C. E. Cann, Description of a prototype emission-transmission CT imaging system. *J Nucl Med*. **33**, pp. 1881-1887, 1992.
17. A. J. Da Silva, H. R. Tang, K. H. Wong, M. C. Wu, M. W. Dae, B. H. Hasegawa, Absolute quantification of regional myocardial uptake of technetium-99m-labeled sestamibi with SPECT: experimental validation in a porcine model. *J Nucl Med*. **42**, pp. 772-779, 2001.
18. H. R. Tang, A. J. Da Silva, K. K. Matthay, D. C. Price, J. P. Huberty, R. A. Hawkins, B. H. Hasegawa, Neuroblastoma imaging using a combined x-ray CT scanner-scintillation camera and iodine-131-labeled metaiodobenzylguanidine (mIBG). *J Nucl Med*. **42**, pp. 237-247, 2001.
19. D. Townsend, P. Kinahan, T. Beyer, Attenuation correction for a combined 3D PET/CT scanner. *Physica Medica*. **12** (Suppl 1), pp. 43-48, 1996.
20. D. W. Townsend, T. Beyer, P. E. Kinahan, A. Brun, R. Roddy, R. Nutt, L. G. Byars, The SMART scanner: a combined PET/CT tomograph for clinical oncology. *Conference Record of the 1998 IEEE Nuclear Science Symposium and Medical Imaging Conference*. **2**, pp. 1170-1174, 1998.
21. P. E. Kinahan, D. W. Townsend, T. Beyer, D. Sashin, Attenuation correction for a combined 3D PET/CT scanner. *Med Phys*. **25**, pp. 2046-2053, 1998.
22. T. Beyer, D. W. Townsend, T. Brun, P. E. Kinahan, M. Charron, R. Roddy, J. Jerin, J. Young, L. Byars, R. Nutt, A combined PET/CT scanner for clinical oncology. *J Nucl Med*. **41**, pp. 1369-1379, 2000.
23. J. A. Patton, D. Delbeke, M. P. Sandler, Image fusion using an integrated, dual-head coincidence camera with x-ray tube-based attenuation maps. *J Nucl Med*. **41**, pp. 1364-1368, 2000.
24. D. Delbeke, W. Hopper, R. Cerci, W. H. Martin, J. A. Patton, M. P. Sandler, Value of attenuation correction and image fusion for interpretation of FDG images using an integrated hybrid camera with x-ray based attenuation maps in patients with known or suspected malignancies. *J Nucl Med*. **41**, pp. 282P, 2000.
25. M. Bocher, A. Balan, Y. Krausz, Y. Shrem, A. Lonn, M. Wilk, R. Chisin, Gamma camera mounted anatomical x-ray tomography: technology, system characteristics, and first images. *Eur J Nucl Med*. **27**, pp. 619-627, 2000.
26. Y. Shao, S. R. Cherry, K. Farahani, R. Slates, Development of a PET detector system compatible with MRI/NMR systems. *IEEE Trans Nucl Sci*. **44**, pp. 1167-1171, 1996.
27. Y. Shao, S. R. Cherry, K. Farahani, K. Meadors, S. Siegel, R. W. Silverman, P. K. Marsden, Simultaneous PET and MR imaging. *Phys Med Biol*. **42**, pp. 1965-1970, 1997.
28. R. Slates, S. Cherry, A. Boutefnouchet, Y. Shao, M. Dahlbom, K. Farahani, Design of a small animal MR compatible PET scanner. *IEEE Trans Nucl Sci*. **46**, pp. 565-570, 1999.
29. R. B. Slates, K. Farahani, Y. Shao, P. Marsden, J. Taylor, P. E. Summers, S. Williams, J. Beech, S. R. Cherry, A study of artifacts in simultaneous PET and MR imaging using a prototype MR compatible PET scanner. *Phys Med Biol*. **44**, pp. 2015-2027, 1999.

30. A. Goertzen. Design of a Simultaneous Combined PET-CT Imaging System for Mouse Imaging. in *HiRes 2001: High Resolution Imaging in Small Animals: Instrumentation, Applications and Animal Handling, September 9-11, 2001*. Rockville MD, 2001.
31. M. Khodaverdi, F. Pauli, S. Weber, G. Schroder, K. Ziemons, R. Sievering, H. Halling, Preliminary studies of a micro-CT for a combined small animal PET/CT scanner. *Conference Proceedings of the IEEE Nuclear Science Symposium and Medical Imaging Conference`*, 2001, *in press*.
32. M. B. Williams, Z. Guimin, M. J. More, A. R. Goode, S. Majewski, R. F. Wojcik, B. Kross, V. Popov, A. G. Weisenberger, M. J. Stanton, W. C. Phillips, A. X. Stewart, T. G. McCauley, W. Tau, E. V. R. Dibella, Integrated CT-SPECT system for small animal imaging. *Proc SPIE: Penetrating radiation systems and applications II*. **4142**, pp. 265-274, 2000.
33. K. Iwata, A. B. Hwang, M. C. Wu, H. R. Tang, A. J. Da Silva, K. H. Wong, M. W. Dae, B. H. Hasegawa, Design and utility of a small animal CT/SPECT system. *Conf Rec 2001 IEEE Nucl Sci Symp Med Imag Conf*., 2001, *in press*.
34. B. H. Hasegawa, B. Stebler, B. K. Rutt, A. Martinez, E. L. Gingold, C. Barker, K. G. Faulkner, C. E. Cann, D. P. Boyd, A prototype high-purity germanium detector system with fast photon-counting circuitry for medical imaging. *Med Phys*. **18**, pp. 900-909, 1991.
35. T. F. Lang, B. H. Hasegawa, S. C. Liew, J. K. Brown, S. Blankespoor, S. M. Reilly, E. L. Gingold, C. E. Cann. A prototype emission-transmission imaging system. in *IEEE Medical Imaging Conference*. Santa Fe, NM: IEEE. **3**, pp. 1902-1906, 1991.
36. K. Kalki, J. A. Heanue, S. C. Blankespoor, X. Wu, J. K. Brown, C. E. Cann, B. H. Hasegawa, J. A. Carver, M. W. Dae, M. Chin, C. Stillson, A combined SPECT and CT medical imaging system. *Proc SPIE*. **2432**, pp. 367-375, 1995.
37. A. R. Goode, M. B. Williams, P. U. Simoni, V. Galbis-Reig, S. Majewski, A. G. Weisenberger, R. Wojcik, M. Stanton, W. C. Phillips, A. X. Stewart, A system for dual-modality breast imaging. *Conf Rec 1999 IEEE Nucl Sci Symp Med Imag Conf*. **2**, pp. 934-938, 1999.
38. K. J. LaCroix, B. M. W. Tsui, B. H. Hasegawa, J. K. Brown, Investigation of the use of x-ray CT images for attenuation correction in SPECT. *IEEE Trans Nucl Sci*. **41**, pp. 2793-2799, 1994.
39. S. Perring, Q. Summers, J. Fleming, M. Nassim, S. Holgate, A new method of quantification of the pulmonary regional distribution of aerosols using combined CT and SPECT and its application to nedocromil sodium administered by metered dose inhaler. *Brit J Radiol*. **67**, pp. 46-53, 1994.
40. R. J. Jaszczak, K. L. Greer, C. E. Floyd, Improved SPECT quantification using compensation for scattered photons. *J Nucl Med*. **25**, pp. 893-900, 1984.
41. K. F. Koral, F. M. Swailem, N. H. Buchbinder, N. H. Clinthorne, W. L. Rogers, B. M. W. Tsui, SPECT dual-energy-window Compton correction: Scatter multiplier required for quantification. *J Nucl Med*. **31**, pp. 90-98, 1990.
42. M. Ljungberg, M. A. King, G. J. Hademenos, S. E. Strand, Comparison of four scatter correction methods using Monte Carlo simulated source distributions. *J Nucl Med*. **35**, pp. 143-151, 1994.
43. M. A. King, G. J. Hademenos, S. J. Glick, A dual-photopeak window scatter correction method. *J Nucl Med*. **33**, pp. 605-613, 1992.
44. T. Mukai, J. M. Links, K. H. Douglass, H. N. Wagner, Scatter correction in SPECT using non-uniform attenuation data. *Phys Med Biol*. **33**, pp. 1129-1140, 1988.
45. P. Msaki, B. Axelsson, S. A. Larsson, Some physical factors influencing the accuracy of convolution scatter correction in SPECT. *Phys. Med. Biol.* **34**, pp. 283-298, 1989.
46. M. Ljungberg, S. Strand, Attenuation correction in SPECT based on transmission studies and Monte Carlo simulations of build-up functions. *J Nucl Med*. **31**, pp. 493-500, 1990.
47. M. Ljungberg, S. E. Strand, Attenuation and scatter correction in SPECT for sources in a nonhomogeneous object: a Monte Carlo study. *J Nucl Med*. **32**, pp. 1278-1284, 1991.
48. E. C. Frey, B. M. W. Tsui. A new method for modeling the spatially-variant, object-dependent scatter response function in SPECT. in *Conf Record IEEE Nucl Sci Symp Med Imag Conf*. Anaheim CA: IEEE, 1996.
49. A. V. Clough, A mathemetical model of single-photon emission computed tomography, in *Optical Sciences*, University of Arizona: Tucson AZ, 1986.
50. W. Nelson, H. Hirayama, D. Rogers, The EGS4 Code System, Stanford Linear Accelerator (Stanford, CA), 1985.

51. R. M. Kessler, J. R. Ellis, M. Eden, Analysis of emission tomographic scan data: Limitations imposed by resolution and background. *J Comput Assist Tomogr*. **8**, pp. 514-522, 1984.
52. H. R. Tang, *A combined x-ray CT-scintillation camera system for measuring radionuclide uptake in tumors*, Doctoral Thesis. Joint Bioengineering Graduate Group, University of California: San Francisco and Berkeley, 1998.
53. A. R. Formiconi, Least squares algorithm for region-of-interest evaluation in emission tomography. *IEEE Trans Med Imag*. **12**, pp. 90-100, 1993.
54. A. Liu, L. E. Williams, A. A. Raubitschek, A CT assisted method for absolute quantitation of internal radioactivity. *Med Phys*. **23**, pp. 1919-1228, 1996.
55. R. E. Carson, A maximum likelihood method for region-of-interest evaluation in emission tomography. *J Comput Assist Tomogr*. **100**, pp. 654-663, 1986.
56. A. Bernstein, M. Breitman, Genetic ablation in transgenic mice. *Molecular Biol Med*. **6**, pp. 523-530, 1989.
57. D. Hanahan, Transgenic mice as probes into complex systems. *Science*. **246**, pp. 1265-1275, 1989.
58. X. Gao, A. Kemper, B. Popko, Advanced transgenic and gene-targeting approaches. *Neurochem Res*. **24**, pp. 1181-1188, 1999.
59. R. Brusa, Genetically modified mice in neuropharmacology. *Pharmacol Res*. **39**, pp. 405-419, 1999.
60. J. N. Crawley, Behavioral phenotyping of transgenic and knockout mice: experimental design and evaluation of general health, sensory functions, motor abilities, and specific behavioral tests. *Brain Res*. **835**, pp. 18-26, 1999.
61. U. Rudolph, H. Mohler, Genetically modified animals in pharmacological research: future trends. *Europ J Pharmacol*. **375**, pp. 327-337, 1999.
62. G. E. Homanics, J. J. Quinlan, R. M. Mihalek, L. L. Firestone, Alcohol and anesthetic mechanisms in genetically engineered mice. *Front Biosci*. **8**, pp. D548-D558, 1998.
63. J. L. Viney, Transgenic and gene knockout mice in cancer research. *Cancer Metast Rev*. **14**, pp. 77-90, 1995.
64. K. D. Becker, K. R. Gottshall, K. R. Chien, Strategies for studying cardiovascular phenotypes in genetically manipulated mice. *Hypertension*. **27**, pp. 495-501, 1996.
65. J. F. James, T. E. Hewett, J. Robbins, Cardiac physiology in transgenic mice. *Circ Res*. **82**, pp. 407-415, 1998.
66. G. Christensen, Y. Wang, K. R. Chien, Physiological assessment of complex cardiac phenotypes in genetically engineered mice. *Am J Physiol*. **227**, pp. H2513-H2524, 1997.
67. M. P. Tornai, R. J. Jaszczak, T. G. Turkington, R. E. Coleman, Small-animal PET: Advent of a new era of PET research (editorial). *J Nucl Med*. **40**, pp. 1176-1179, 1999.
68. M. E. Phelps, J. C. Mazziotaa, H. R. Schelbert, *Positron emission tomography and autoradiography: Principles and Applications for the Brain and Heart*, New York: Raven Press, c. 1986.
69. S. S. Gleason, H. Sari-Sarraf, M. J. Paulus, D. K. Johnson, Reconstruction of multi-energy x-ray computed tomography of laboratory mice. *IEEE Trans Nucl Sci*. **46**, pp. 1081-1086, 1999.
70. M. J. Paulus, H. Sari-Sarraf, S. S. Bleason, M. Bobrek, A new x-ray computed tomography system for laboratory mouse imaging. *IEEE Trans Nucl Sci*. **46**, pp. 558-564, 1999.
71. S. Siegel, J. J. Vaquero, L. Aloj, J. Seidel, Initial results from a PET/planar small animal imaging system. *IEEE Trans Nucl Sci*. **46**, pp. 571-575, 1998.
72. S. R. Meikle, S. Eberl, R. R. Fulton, M. Kassiou. The influence of tomograph sensitivity on parameter estimation in small animal imaging studies. in *1998 IEEE Nuclear Science Symposium and Medical Imaging Conference*. Toronto ON. **3**, pp. 1898-1903, 1989.
73. J. A. Correia, C. A. Burnham, D. Kaufman, A. J. Fischman, Development of a small animal PET imaging device with resolution apporaching 1 mm. *IEEE Trans Nucl Sci*. **46**, pp. 631-635, 1999.
74. R. S. Miyaoka, T. K. Lewellen. Design analysis of a high resolution detector block for a low cost small animal positron imaging system. in *1994 IEEE Nuclear Science Symposium and Medical Imaging Conference*. Norfolk VA. **3**, pp. 1370-1374, 1994.
75. S. R. Cherry, Y. Shao, R. W. Silverman, K. Meadors, MicroPET: a high resolution PET scanner for imaging small animals. *IEEE Trans Nucl Sci*. **44**, pp. 1161-1166, 1997.
76. J. S. Fowler, N. D. Volkow, G. J. Wang, Y. S. Ding, S. L. Dewey, PET and drug research and development. *J Nucl Med*. **40**, pp. 1154-1163, 1999.
77. R. J. Jaszczak, J. Li, H. Wang, M. R. Zalutsky, R. E. Coleman, Pinhole collimation for ultra high-resolution, small field of view SPECT. *Phys Med Biol*. **39**, pp. 425-437, 1994.
78. S. E. Strand, M. Ivanovic, K. Erlandsson, D. Franceschi, T. Burton, K. Sjogren, D. A. Weber, Tumor imaging with pinhole SPECT. *Cancer*. **73** (suppl), pp. 981-984, 1994.

79. J. Li, R. J. Jaszczak, K. L. Greer, R. E. Coleman, A filtered backprojection algorithm for pinhole SPECT with a displaced center of rotation. *Phys Med Biol*. **39**, pp. 165-176, 1994.
80. E. L. Johnson, T. G. Turkington, R. J. Jaszczak, D. R. Gilland, G. Vaidyanathan, K. L. Greer, R. E. Coleman, M. R. Zalutsky, Quantitation of 211At in small volumes for evaluation of targeted radiotherapy in animal models. *Nucl Med Biol*. **22**, pp. 45-54, 1995.
81. D. A. Weber, M. Ivanovic, Pinhole SPECT: ultra-high resolution imaging for small animal studies. *J Nucl Med*. **36**, pp. 2287-2289, 1995.
82. D. A. Weber, M. Ivanovic, Ultra-high-resolution imaging of small animals: implications for Gpreclinical and research studies. *J Nucl Cardiol*. **6**, pp. 332-344, 1999.
83. K. Ishizu, T. Mukai, Y. Yonekura, M. Pagani, Ultra-high resolution SPECT system using four pinhole collimators for small animal studies. *J Nucl Med*. **36**, pp. 2282-2286, 1995.
84. K. Ogawa, T. Kawade, K. Nakamura, A. Kubo, Ultra high resolution pinhole SPECT for small animal study. *IEEE Trans Nucl Sci*. **45**, pp. 3122-3126, 1998.
85. H. B. Barber, B. A. Apotovsky, F. L. Augustine, H. H. Barrett, Semiconductor pixel detectors for gamma-ray imaging in nuclear medicine. *Nucl Instru Meth Phys Res A*. **395**, pp. 421-428, 1997.
86. H. B. Barber, D. G. Marks, B. A. Apotovsky, F. L. Augustine, Progress in developing focal-plane-multiplexer readout for large CdZnTe arrays for nuclear medicine applications. *Nucl Instr Method Phys Res A*. **380**, pp. 262-265, 1996.
87. A. G. Weisenberger, R. F. Wojcik, P. Bradley, S. Brewer, S. Majewski, J. Qian, A. Ranck, K. Saha, M. F. Smith, R. E. Welsh, SPECT-CT system for small animal imaging. *Conf Rec 2001 IEEE Nucl Sci Symp Med Imag Conf*., 2001, *in press*.
88. L. R. MacDonald, B. E. Patt, J. S. Iwanczyk, B. M. W. Tsui, Y. Wang, E. C. Frey, D. E. Wessell, P. D. Acton, H. F. Kung, Pinhole SPECT of mice using the LumaGEM gamma camera. *IEEE Trans Nucl Sci*. **48**, pp. 830-836, 2001.
89. D. P. McElroy, L. R. MacDonald, F. J. Beekman, Y. Wang, B. E. Patt, J. S. Iwanczyk, B. M. W. Tsui, E. J. Hoffman, Evaluation of A-SPECT: A desktop pinhole SPECT system for small animal imaging, 2002, *submitted for publication*.
90. K. Iwata, M. C. Wu, B. H. Hasegawa, X-ray CT and SPECT systems for small animals. *Conf Rec 1999 IEEE Nucl Sci Symp Med Imag Conf*. **3**, pp. 1318-1322, 1999.
91. M. Ding, A. Odgaard, I. Hvid, Accuracy of cancellous bone volume fraction measured by micro-CT scanning. *J Biomech*. **32**, pp. 323-326, 1999.
92. E. L. Ritman, M. E. Bolander, L. A. Fitzpatrick, R. T. Turner, Micro-CT imaging of structure-to-function relationship of bone microstructure and associated vascular involvement. *Technol Health Care*. **6**, pp. 403-412, 1998.